COMMUNICATIONS CHEMISTRY

ARTICLE

https://doi.org/10.1038/s42004-019-0195-3 OPEN

Green fabrication of stable lead-free bismuth based perovskite solar cells using a non-toxic solvent

Sagar M. Jain[1], Tomas Edvinsson[2] & James R. Durrant[1,3]

The very fast evolution in certified efficiency of lead-halide organic-inorganic perovskite solar cells to 24.2%, on par and even surpassing the record for polycrystalline silicon solar cells (22.3%), bears the promise of a new era in photovoltaics and revitalisation of thin film solar cell technologies. However, the presence of toxic lead and particularly toxic solvents during the fabrication process makes large-scale manufacturing of perovskite solar cells challenging due to legislation and environment issues. For lead-free alternatives, non-toxic tin, antimony and bismuth based solar cells still rely on up-scalable fabrication processes that employ toxic solvents. Here we employ non-toxic methyl-acetate solution processed $(CH_3NH_3)_3Bi_2I_9$ films to fabricate lead-free, bismuth based $(CH_3NH_3)_3Bi_2I_9$ perovskites on mesoporous TiO_2 architecture using a sustainable route. Optoelectronic characterization, X-ray diffraction and electron microscopy show that the route can provide homogeneous and good quality $(CH_3NH_3)_3Bi_2I_9$ films. Fine-tuning the perovskite/hole transport layer interface by the use of conventional 2,2′,7,7′-tetrakis (*N*,*N*′-di-*p*-methoxyphenylamino)−9,9′-spirbiuorene, known as Spiro-OMeTAD, and poly(3-hexylthiophene-2,5-diyl - P3HT as hole transporting materials, yields power conversion efficiencies of 1.12% and 1.62% under 1 sun illumination. Devices prepared using poly(3-hexylthiophene-2,5-diyl hole transport layer shown 300 h of stability under continuous 1 sun illumination, without the use of an ultra violet-filter.

[1] SPECIFIC, College of Engineering, Swansea University Bay Campus, Fabian Way, SA1 8EN Swansea, UK. [2] Department of Engineering Sciences, Solid State Physics, Uppsala University, Box 534, SE 751 21 Uppsala, Sweden. [3] Department of Chemistry and Centre for Plastic Electronics, Imperial College London, Exhibition Road, London SW7 2AZ, UK. Correspondence and requests for materials should be addressed to S.M.J. (email: sagarmjain@gmail.com)

Organic–inorganic, lead-halide-based perovskite solar cells (PSCs) have recently emerged as a very promising photovoltaic system with certified solar cell performance surpassing 24% [https://www.nrel.gov/pv/assets/images/efficiency-chart-20180716.jpg].

Lead-based perovskites for solar cells are commonly prepared into polycrystalline films with a local 3D crystal structure with a stoichiometry of ABX_3. Where, A is the cation (methylamine, formamide or caesium), B is second cation, either lead or tin and the X anion is a halide, such as chlorine, bromine or iodine. Recent high efficiency perovskite absorbers have a mixture of multiple ions at the A and X sites [1–4].

The large possibilities in elemental composition and local arrangements of cations allow fine-tuning of the optoelectronic properties of the perovskite absorber, where the high-yield performance and band gap tuning make them promising in both single-junction devices and multi-junction tandem applications. Solution processing of these solar cells potentially allows low cost, large-scale manufacturing, possibly providing an alternative to crystalline silicon, CdTe or CIGS solar cells, or as a potentially cheap tandem material to be used in a hybrid tandem solar cell together with conventional PV technology. For the transformation of lab-scale perovskite devices to real-world deployment, the toxicity of these materials (lead content) and toxic solvents such as dimethylformamide (DMF), dimethyl sulfoxide (DMSO) and gamma butyrolactone (GBL) used remain an inevitable issue to be solved for their large-scale production[5]. In addition, a flexibility on replacing a toxic solvent would broaden the possibilities for compatibility of hybrid perovskite technologies if incorporated in already developed synthesis routes for sensors and solar cells where solvents otherwise could dissolve already applied materials.

Sources of toxicity for these solar cells can be distinguished into two categories: (1) the inherent toxicity of the water-soluble lead salt present, and (2) the toxic solvents used in the manufacture of devices, such as dimethylformamide (DMF), dimethyl sulfoxide (DMSO), gamma butyrolactone (GBL), chlorobenzene and toluene. These solvents have low exposure limits, and are not compatible with low cost, large-scale printing techniques in an ambient environment. To avoid the health hazards involved by contact with toxic lead as well as toxic solvent inhalation during large-scale manufacturing, research is beginning to address these key barriers with several reports on lead-free perovskite materials and 'greener solvents' toxic-free approaches.

The presence of lead in perovskite in water-soluble form remains an environmental and health concern. This issue is well acknowledged within the scientific community, and a large amount of research is directed to fabrication and investigations of lead-free perovskite solar cell materials employing tin (Sn), bismuth (Bi) or antimony (Sb) as a substitute for toxic lead (Pb)[6–19]. Power-conversion efficiency (PCE) for lead-free, tin-based $FASnI_3$ perovskites presently shows 9% record PCE[20]. One remaining concern, however, is that they suffer from notorious problem of rapid oxidation of Sn^{2+} to Sn^{4+} resulting into the rapid degradation in ambient environment[21,22]. Another is that the lower electron density that can be polarised in the Sn halide perovskite, compared with the Pb-analogue, produce a less sharp absorption onset at the band gap limit, lower the total number of photogenerated charges in the region close to the band gap. Here, Bi has a more stable oxidation number and share a similar polarisable electron density as Pb.

Binary PSCs with silver in the structure, Ag_3BiI_6 and $AgBiI_7$, have achieved PCEs of 4.1% and 1.22%, respectively. Since Ag has a strong affinity for halide, the formation of AgI in these solar cells leads to problems with the inherent stability under illumination and increase in hygroscopic nature of the absorber layer that is detrimental for the stability of devices [23,24].

In contrast to tin-based and binary cation perovskite, antimony and bismuth-based perovskite-like materials are highly stable in ambient atmosphere and possess exceptional optoelectronic properties[25]. These have recently been used as a lead-free absorber in PSCs[25–30]. To some extent, antimony shares the less sharp onset of absorption as the tin-based systems. For silver-free bismuth-based perovskite-like MBI ($CH_3NH_3Bi_2I_9$) absorber in FTO/c-TiO_2/Meso-TiO_2/MBI/P3HT/Au architecture, a world record, hysteresis-free, PCE of 3.17% was recently reported[28]. The improved performance was achieved as a result of the formation of high-quality MBI absorber film with vapour saturation. Although the replacement of toxic lead is well addressed, there is still lack of methods employing non-toxic solvent routes during the fabrication process of the PSCs that show same or improved performance. For instance, all the above lead-free solar cells[6–19,26–31], still employ DMF, DMSO or GBL toxic solvents as well as toxic antisolvents having low exposure limits for forming high-quality perovskite-like crystalline material. In this direction of the use of green, more environmental friendly solvents, Noel et al. reported the use of less toxic acetonitrile solvent for the fabrication of lead-based PSCs and achieved an impressive PCE of 19%[32]. Although less toxic than some alternative solvents, acetonitrile is still carcinogenic and demands protection of workspace and personnel. Galagan et al.[33] reported industrially compatible solvent for preparation of efficient lead-based solar cells.

Here, we describe the use of the non-toxic solvent methyl-acetate to fabricate lead-free MBI perovskite on FTO/c-TiO_2/Meso-TiO_2 architecture. The selection of appropriate hole transport materials, conventional (2,2′,7,7′-tetrakis (*N*,*N*′-di-*p*-methoxyphenylamino)-9,9′-spirbiuorene) (Spiro-OMeTAD) and poly(3-hexylthiophene-2,5-diyl (P3HT) yields devices with efficiency of 1.12% and 1.62%, respectively, in toxic lead and solvent-free solar cells.

In addition, we have avoided the use of silver or gold as a counter metal electrode in the fabrication of the solar cells. These changes are employed taking in account the detrimental effect of metal electrodes infiltration into perovskite causing degradation of solar devices[34,35]. For the same reason as well as for lowering the material cost, a more stable, hydrophobic carbon paste is used as counter electrode anticipated to improve long-time stability.

Results

Optoelectronic and crystalline properties of the non-toxic MBI film. The light-absorbing film is made from powder CH_3NH_3I (MAI) and BiI_3 salts in a 1:1.7 molar ratio, dissolved in 1 ml of methyl-acetate following the detailed experimental procedure mentioned earlier. The saturated solution of MBI is spin coated on the FTO/mesoporous-TiO_2 substrate. X-Ray diffraction and scanning electron microscopy were used to characterise the crystal structure, phase purity and surface morphology of the prepared films.

The XRD pattern in Fig. 1a shows distinct peak at 12.5°, 14.6°, 17.0°, 25.3°, 26.9° and 29° theta angle indicating (003), (102), (103), (006), (203), (204) and (205), respectively, compatible with a single-crystalline phase and an indication of formation of high-quality MBI films[36]. These results are also confirmed from the large crystal grains as observed from surface morphology micrographs of the film (Supplementary Fig. 1).

The absence of peak at 9°, 19° and 29° indicates absence of MAI crystallisation in perovskite films, supporting a conversion of the precursor materials into MBI films[37–39]. The MBI crystal belongs to the hexagonal system with (P1 21 1) space group. Figure 1b represents the 3D crystal structure of MBI viewed from front and side angles. Figure 1c shows reflectance spectra of the MBI film (with satellite image—orange colour film), from

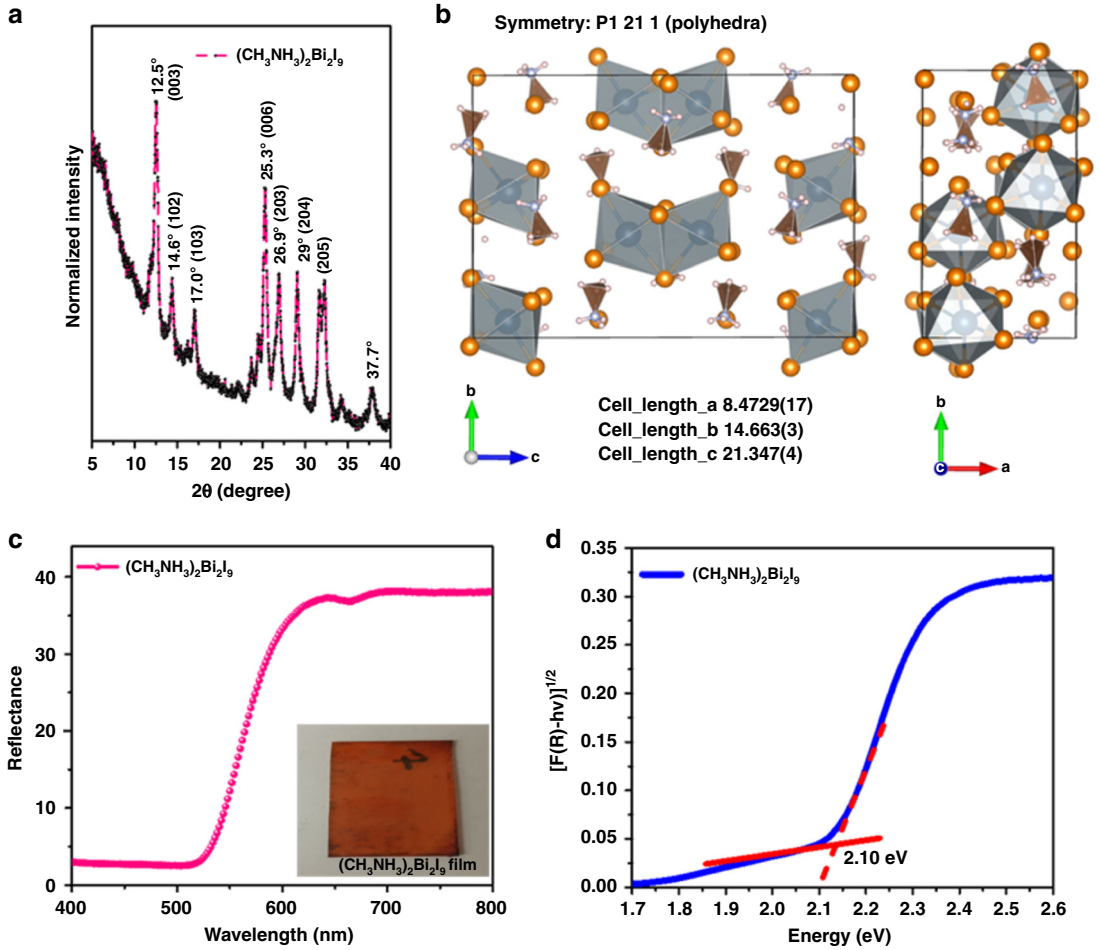

Fig. 1 Crystalline and optical characteristics of MBI films. **a** X-ray diffraction pattern. **b** Three-dimensional crystal structure of the MBI viewed from different directions. **c** Reflectance spectrum. Inset is the picture of the MBI film. **d** Calculated spectrum of the MBI film deposited on the Glass/Meso-TiO_2 substrate

reflectance spectra and Kuble–Kamunk measurements band gap is calculated for the MBI film, which is ~2.1 eV. Close match to the single crystal of MBI perovskite and valence band cut-off of the film.

Optoelectronic properties of MBI films were probed using absorbance, steady-state and time-resolved photoluminescence spectroscopy. MBI films deposited directly on glass substrate were used for the measurements. MBI films deposited by using methyl-acetate solution shows substantially reduced excitonic peak with the absorbance from 350 to 600 nm. This reduced intensity of excitonic peak which is observed at $absorbance_{maxima} = 500$ nm[28] is a good indication of loosely bound excitons, compatible with large crystallites and a 3D structured perovskite-like film. Figure 2b black spectrum shows steady-state PL of pristine MBI films deposited on the glass substrate. The high PL intensity further supports the formation of a good quality MBI films. Spin coating, the HTM layer on top of the MBI films and measuring the steady-state PL, shows the expected quenching of the PL intensity upon charge transfer. The PL intensity for the MBI/P3HT films is strongly quenched (43%) and confirms that efficient charge separation occurrs at the MBI/P3HT interface, but also that a portion underneath this layer is not fully charge quenched. The PL quenching is further confirmed from the time-correlated single-photon counting measurements (Fig. 2c).

Supplementary Figure 3 shows X-ray photoelectron spectroscopy (XPS) Bi *4f* and I *3d* core-level experimental spectra for MBI films deposited on TiO_2 substrate. Photon energy of 4000 eV is used, enabling >20 nm depth penetration and therefore detects more bulk-like properties of the samples via the core-level spectra reported here. This is important, as the surface states can be strongly affected by the history of the samples, the conditions and surface exposures used during the measurements, and eventually, by the type and process used when adding the final charge-selective material.

The core-level spectra Bi *4f* shown a peak at 158 eV, indicative of the Bi present in Bi^{3+} oxidation state[28]. The iodine 3*d* core-level peaks found around a binding energy of 620 nm. Indicating the anion isoelectronic iodine environment. The experimental valence band spectra for MBI films are shown in Supplementary Figure 3c. The valance band offset is at ≈1.5 eV.

Photovoltaic characteristics of non-toxic MBI PSCs. The energy levels for TiO_2, P3HT and carbon are taken from previous references[28,40,41], as shown in Supplementary Table 2.

The X-ray diffraction, surface morphology, X-ray photoelectron spectroscopy (Supplementary Fig. 3) and optoelectronic characterisation show and confirm the formation of high-quality MBI films formed employing methyl-acetate as a non-toxic solvent system.

From the application point of view and to validate the influence of these films when applied as the absorber layer in solar cells, we fabricated solar cells on FTO substrates with a compact TiO_2 and an additional layer of mesoporous-TiO_2 prepared by spray pyrolysis and spin coating, respectively. Further materials were propped to fine tune the MBI/HTM interface and also to validate the applicability of the new solvent

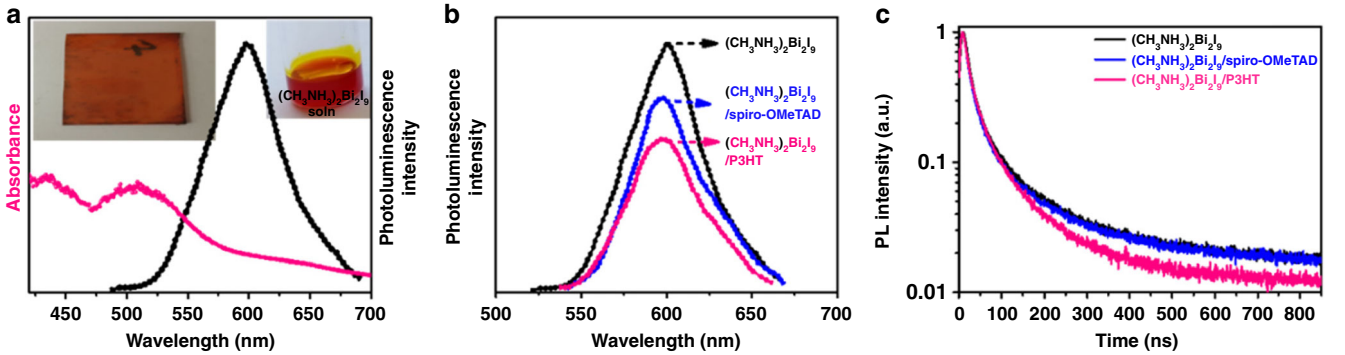

Fig. 2 Optoelectronic characteristics of MBI films. **a** Absorbance and photoluminescence spectrum. Right hand side and left hand side inset is picture of MBI solution and film, respectively. **b** Steady-state photoluminescence measured on bare perovskite film (black) and hole transport layer (HTL) deposited on the perovskite. Black and blue curves represent Spiro-OMeTAD and P3HT deposited on perovskite, respectively. **c** Time-resolved photoluminescence taken at excitation wavelength of 525 nm of the perovskite films with different HTLs

route, two different HTMs, Spiro-OMeTAD and P3HT (poly (3-hexylthiophene-2,5-diyl) commonly used as P-type contacts for organic or hybrid solar cells. The role of HTM is effectively collect holes blocking electron and thus avoiding charge recombination. In addition, hole transport material (HTM) could act as shielding hydrophobic encapsulating layer for the underneath moisture-sensitive absorber layer avoiding degradation from external factors (moisture, temperature and light). The surface morphology and cross-section of the solar cell are shown in Supplementary Fig. 1. Device cross-section shows thicker ≈600 nm MBI absorber films with improved crystalline quality formed using methyl-acetate solution as confirmed from the X-ray diffraction measurements and also when employed shows improved device performance.

Figure 3b and Table 1 show *JV* characteristics of solar cells prepared using MBI as an active layer and conventional Spiro-OMeTAD (2,2′,7,7′-tetrakis(*N*,*N*′-di-*p*-methoxyphenylamino)-9,9′-spirbiuorene) and P3HT as a HTMs shows hysteresis-free, current–voltage curves and PCE of 1.12% and 1.62%, respectively (Supplementary Fig. 4, Supplementary Table 1). The solar cells prepared with P3HT as hole-transport layer shows the champion performance of 1.62% ($Voc = 0.87$ V, $Jsc = 2.70$ mA/cm^2 and $FF = 0.69$) as a result of enhanced hole-transport properties across MBI/P3HT interface due to matching energy levels at the interface. The cells with Spiro-OMeTAD show the relatively lower PCE of 1.12% ($Voc = 0.76$ V, $Jsc = 2.75$ mA/cm^2 and $FF = 0.54$). The improved performance from 1.12% to 1.62% is mainly from the enhanced *Voc* from 0.76 V to 0.87 V, and can be attributed to a more deep HOMO level of P3HT (−3.5 eV) as compared with Spiro-OMeTAD (−2.22)[42] that blocks holes more efficiently and leads to improved *Voc* for the PSCs made using P3HT hole transport layer (HTL). Moreover, the *Voc* originates in the difference in the quasi Fermi levels at each side of the device and relates to the respective energy levels[39,43–46], as well as recombination rate[47] and density of states disorder[48,49]. The EQE curve covers 23% of the total spectrum and the calculated photocurrent density from EQE of 2.70 mA/cm^2, which is well match to the current density obtained from *JV* curves. The performance statistics of 27 solar cells prepared using each Spiro-OMeTAD and P3HT HTL (Supplementary Fig. 5) shows average device efficiency of 1.0% and 1.4% for devices prepared using Spiro-OMeTAD and P3HT HTL, respectively.

Stability of lead-free solar cells is an important aspect. We have subjected the non-encapsulated MBI solar cells fabricated using P3HT and Spiro-OMeTAD as HTLs to continuous 1 sun (100 mW/cm^2, AM 1.5) illumination without use of UV-filters for 840 h (35 days) and monitored the performance. BiI_3 have lower water solubility as compared with PbI_2, this eventually benefits for improving the stability as well has advantage of lowering toxicity effect for the bismuth-based solar cells. Although solar cells are expected to be encapsulated in a final applications, the non- encapsulated solar cells give an accelerated test of either intrinsic instabilities or long-term leakage of moisture or/and oxygen into the encapsulation. Both the solar cells shows initial increase in efficiency from 0.5 to 1%, this might be as an effect of light soaking. The perovskite cells made employing Spiro-OMeTAD HTM undergone rapid degradation reducing the PCE from 1.12% to 0.7% in only 245 h (10 days) of illumination time. While, the devices prepared using P3HT HTM have shown long-sustained stability, reducing PCE from 1.6% to 1.4% only, i.e., negligible drop of 0.2% in PCE. To further illustrate the reason of degradation of solar cells, we performed stability test on the sample prepared with FTO/TiO_2/MBI architecture. With light soaking of MBI films with 1 sun illumination over extended period of time (30 days = 720 h) and monitored the changes with X-ray diffraction measurements (Supplementary Fig. 2), the MBI films showed no trace of degradation of the crystalline quality. This confirms that the degradation is caused at the Spiro/MBI interface as a result of more hygroscopic nature of Spiro-OMeTAD as compare with the P3HT[42,50]. In our previous study, we have shown the notorious, degradation susceptible behaviour of doped Spiro-OMeTAD HTM reflected in the degradation of PSCs. Tailoring the energy level of HTLs and electron transport layers (ETLs) to match better with that of the perovskite layer can improve electron and hole extraction and transport, contributing to the increase of *Jsc* and *FF*. Particularly, the poor *Voc* of $CH_3NH_3BiI_3$ can be improved by the minimising energy difference between the Fermi level (E_F) of the ETLs.

Discussion

In this work, we have fabricated a lead-free perovskite solar cell without the use of toxic solvents. The high-quality MBI films were fabricated using methyl-acetate as a non-toxic solvent system. The high quality of the films were confirmed from X-ray diffraction, optoelectronic and X-ray photoelectron spectroscopy characterisation. The devices fabricated with Spiro-OMeTAD and P3HT as the HTL yielded 1.12% and 1.62% efficiency. In addition, a more stable back contacts replacing the unstable silver and expensive gold metal electrodes is employed that adds the additional advantage of improved scalability and lowering of the material costs. The results show that solar cells with MBI/P3HT interface have improved stability, at least when used in non-encapsulated environments. Perovskite solar cell technology is

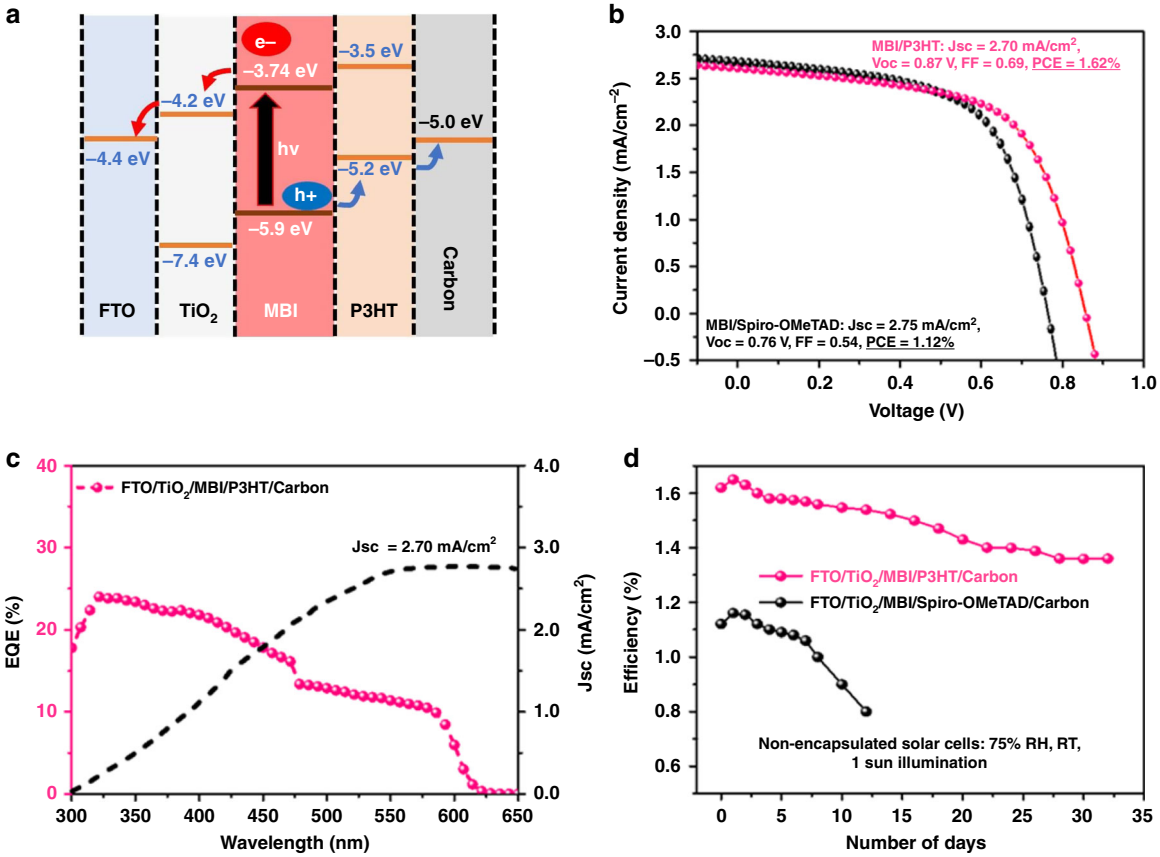

Fig. 3 Photovoltaics performance and stability of non-toxic MBI perovskite solar cells. **a** Energy band levels diagram for device architecture with FTO/TiO_2/MBI ($(CH_3NH_3)_2Bi_2I_9$))/P3HT/Carbon configuration VBM value of MBI is determined by the UPS result, and the CBM value of MBI is calculated based on the optical band gap of the MBI. **b** Photovoltaic performance of optimised champion PSC devices made using different hole transport layers using P3HT (red curve) and Spiro-OMeTAD (black curve) as the hole transporting layers. **c** EQE and integrated photocurrent for champion solar cell made using P3HT hole transport materials. **d** Stability measurements for non-encapsulated solar cells measured at room temperature, the devices were kept under continuous 1 sun illumination

Table 1 Photovoltaic performance parameters for MBI solar cells

Solar cells made with different HTMs	*Jsc* (mA/cm^2)	*Voc* (V)	*FF* (%)	*PCE* (%)
Spiro-OMeTAD	2.75	0.76	0.54	1.12
P3HT	2.70	0.87	0.69	1.62

Jsc short-circuit photocurrent density, *Voc* open-circuit voltage, *FF* fill factor, *PCE* power conversion efficiency
Solar cells made employing different hole transport layers at 1000 Wm^{-2} (AM 1.5 G) measured at constant scan speed of 10 mVs^{-1}

facing major challenges relating to developing non-toxic, large-scale production scheme. The PCEs are in level with the best routes using toxic solvents for bismuth-based perovskites, and may offer a way to a sustainable manufacturing approach for production using non-toxic solvent as well as toxic lead-free PSCs. This study, using an 'all green' approach using a non-toxic solvent and avoiding the use of lead, while yielding crystal qualities and efficiencies on par with previous routes using toxic solvents, may aid scaling up lead and toxic solvent-free technology and thus facilitating its widespread utilisation.

Methods

Fabrication of devices. FTO glass substrates were etched with 2 M HCl and zinc powder washed with IPA, acetone and clean water, and dried before use. The TiO_2 precursor was prepared as reported in ref. [28]. The as-prepared TiO_2 films then spin coated on substrate at 3000 rpm for 30 s and then sintered for 450 °C for 1 h to form a compact layer. A mesoporous-TiO_2 gel was subsequently spin coated on the compact layer at 4000 rpm for 30 s, and then sintered at 500 °C for 30 min. After the substrates cooled down, MAI and BiI_3 salts in variable molar ratios of 1:1.7, 1:1.9, 1:2, 1:2.2, 1:2.4, 1:2.5 and 1:2.6 were dissolved in 1 ml of methyl-acetate solution and sonicated overnight at RT and subsequently heated at 110 °C for 2 h. The solution was then filtered through a 4 -µm filter and spin coated on a FTO/c-TiO_2/mesoporous-TiO_2 substrate at 4000 RPM for 30 s. The films were annealed at 150 °C for 30 min. Only the optimised concentration with molar ration of 1:1.7 that yields the MBI crystal structure (confirmed from X-ray diffraction and X-ray photoelectron spectroscopy measurements) is employed as absorber layer to prepare solar cell devices.

P3HT-poly (3-hexylthiophene-2,5-diyl) (99.9% Sigma-Aldrich) was prepared and deposited as previously described in ref. [28] and used as HTM, and the conventional Spiro-OMeTAD (2,2′,7,7′-tetrakis(*N*,*N*′-di-*p*-methoxyphenylamino)-9,9′-spirbiuorene) was prepared and deposited as described previously[42]. Finally, ≈150 -nm thick carbon paste was applied on the sample to form a counter electrode. The preparation of the solution is made in ambient environment, while the spin-coating procedure is performed in glovebox under controlled humidity and in nitrogen environment.

PCE and incident photon to current conversion efficiency (IPCE). Masked devices (0.125 cm^2) were tested under a class AAA solar simulator (Newport Oriel Sol3A) at 1.5 and 100 mWcm^{-2} illumination conditions calibrated against a KG5 filtered silicon reference cell (Newport Oriel 91150 KG5) using a Keithley

2400 source metre. Current–voltage sweeps were performed forward to reverse at a rate of 10 mV s^{-1}. Stabilised PCE was measured at the maximum power point tracking for 5 min.

Characterisation. All the characterisation tests done on three-layered assembly: Glass/Meso-TiO_2/Perovskite for all samples, in order to mimics the device architecture.

XRD measurements. XRD was performed with a Siemens diffractometer D5000 using CuKα radiation and diffract plus XRD commander software. The instrument was set in 'detector scan' mode, and the acquisition was done in $\Theta-2\Theta$ mode for every 0.02° increment over the Bragg angle range of 10–65°.

UV-visible and photoluminescence measurements. UV-visible and %R measurements were performed using LAMBDA 950 Spectrophotometer from PerkinElmer. %R measurements were performed using integrating sphere and using 0% and 100% baseline correction before measuring the samples. Photoluminescence measurements were performed using Horiba Fluromax-4 spectroflurometer equipped with double grating at the excitation wavelength of 550 nm.

Scanning electron microscopy and EDX measurements. The surface morphology and element analysis of as-prepared samples were done on the scanning electron microscopy (SEM, Zeiss 1550) with AZtec EDS, which were operated at 5–10 -kV accelerating voltage.

X-ray photoelectron spectroscopy measurements. Hard X-ray Photoemission spectroscopy (HAXPES) was performed at BESSY II (Helmholtz Zentrum Berlin) the HIKE end-station[51,52]. The spectra presented were energy calibrated and were intensity normalised using the most intense peak [51,52].

Stability measurements: The champion non-encapsulated devices were tested for stability measurements under continuous 1 sun (AM 1.5 G) illumination at maximum power point for 400 h in ambient air environment, with the performance of the solar cells measured simultaneously. For long-term stability measurements, the devices were kept in ambient air environment and under 1 sun (AM 1.5 G) illuminations for more than 30 days and efficiency measurements carried out manually after regular days interval of exposure to 1 sun illumination. All the stability measurements performed using UV-component of the lamp.

Data availability

All the relevant data are available from the authors upon appropriate request.

Received: 1 March 2019 Accepted: 16 July 2019
Published online: 08 August 2019

References

1. Saliba, M. et al. Incorporation of rubidium cations into perovskite solar cells improves photovoltaic performance. *Science* **354**, 206–209 (2016).
2. Saliba, M. et al. Cesium-containing triple cation perovskite solar cells: improved stability, reproducibility, and high efficiency. *Energy Environ. Sci.* **9**, 1989–1997 (2016).
3. Jeon, N. J. et al. Compositional engineering of perovskite materials for high-performance solar cells. *Nature* **517**, 476–480 (2015).
4. Pellet, N. et al. Mixed-organic-cation perovskite photovoltaics for enhanced solar-light harvesting. *Angew Chem. Int'l Ed.* **53**, 3151–3157 (2014).
5. Babayigit, A., Ethirajan, A., Muller, M. & Conings, B. Toxicity of organometal halide perovskite solar cells. *Nat. Mater.* **15**, 247–251 (2016).
6. Slavney, A. H., Hu, T., Lindenberg, A. M. & Karunadasa, H. I. A bismuth halide double perovskite with long carrier recombination lifetime for photovoltaic applications. *J. Am. Chem. Soc.* **138**, 2138–2141 (2016).
7. Song, T.-B., Yokoyama, T., Aramaki, S. & Kanatzidis, M. G. Performance enhancement of lead-free tin-based perovskite solar cells with reducing atmosphere-assisted dispersible additive. *ACS Energy Lett.* **2**, 897–903 (2017).
8. Chatterjee, S., Bera, A. & Pal, A. J. p-i-n heterojunctions with $BiFeO_3$ perovskite nanoparticles and p- and n-type oxides: photovoltaic properties. *ACS Appl. Mater. Interfaces* **6**, 20479–20486 (2014).
9. Lehner, A. J. et al. Crystal and electronic structures of complex bismuth iodides $A_3Bi_2I_9$ (A = K, Rb, Cs) related to perovskite: aiding the rational design of photovoltaics. *Chem. Mater.* **27**, 7137–7148 (2015).
10. Singh, T., Kulkarni, A., Ikegami, M. & Miyasaka, T. Effect of electron transporting layer on bismuth-based lead-free perovskite $(CH_3NH_3)_3$ Bi_2I_9 for photovoltaic applications. *ACS Appl. Mater. Interfaces* **8**, 14542–14547 (2016).
11. Vigneshwaran, M. et al. Facile synthesis and characterization of sulfur doped low bandgap bismuth based perovskite by soluble precursor route. *Chem. Mater.* **28**, 6436–6440 (2016).
12. Brandt, R. E. et al. Investigation of bismuth triiodide (BiI_3) for photovoltaic applications. *J. Phys. Chem. Lett.* **6**, 4297–4302 (2015).
13. Lyu, M. et al. Organic–inorganic bismuth (III)-based material: a lead-free, air-stable and solution-processable light-absorber beyond organolead perovskites. *Nano Res.* **9**, 692–702 (2016).
14. Sun, S. et al. Synthesis, crystal structure and properties of perovskite-related bismuth phase, $(NH_4)_3Bi_2I_9$. *APL Mater.* **4**, 0311011–0311017 (2016).
15. Kamat, P. V., Bisquert, J. & Buriak, J. Lead free perovskite solar cells. *ACS Energy Lett.* **2**, 904–905 (2017).
16. Tsai, C. M. et al. Role of tin chloride in tin-rich mixed-halide perovskites applied as mesoscopic solar cells with a carbon counter electrode. *ACS Energy Lett.* **1**, 1086–1093 (2016).
17. Saparov, B. et al. Thin-film preparation and characterization of $Cs_3Sb_2I_9$: a lead-free layered perovskite semiconductor. *Chem. Mater.* **27**, 5622–5632 (2015).
18. Wei, F. et al. The synthesis, structure and electronic properties of a lead-free hybrid inorganic–organic double perovskite $(MA)_2KBiCl_6$ (MA=methylammonium). *Mater. Horiz.* **3**, 328–332 (2016).
19. Wang, C. R., Yang, Q., Tang, K. B. & Qian, Y. T. Preparation and vibrational properties of BiI_3 nanocrystals. *Chem. Lett.* **2**, 154–155 (2001).
20. Shao, S. et al. Highly reproducible Sn-based hybrid perovskite solar cells with 9% efficiency. *Adv. Energy Mater.* **8**, 1702019 (2018).
21. Parrott, E. S. et al. Effect of structural phase transition on charge-carrier lifetimes and defects in $CH_3NH_3SnI_3$ perovskite. *J. Phys. Chem. Lett.* **7**, 1321–1326 (2016).
22. Hao, F., Stoumpos, C. C., Cao, D. H., Chang, R. P. H. & Kanatzidis, M. G. Lead-free solid-state organic–inorganic halide perovskite solar cells. *Nat. Photonics* **8**, 489–494 (2014).
23. Kim, Y. et al. Pure cubic-phase hybrid iodobismuthates AgBi2I7 for thin-film photovoltaics. *Angew Chem. Int Edition* **128**, 9738–9742 (2016).
24. Turkevych, I. et al. Photovoltaic rudorffites: lead-free silver bismuth halides alternative to hybrid lead halide perovskites. *Chem. Sus. Chem.* **10**, 1–7 (2017).
25. Lyu, M. et al. Organic–inorganic bismuth (III)-based material: a lead-free, air-stable and solution-processable light-absorber beyond organolead perovskites. *Nano Res.* **9**, 692–702 (2016).
26. Chen, D., Zhou, S., Fang, G., Chen, X. & Zhong, J. Fast room-temperature cation exchange synthesis of Mn-doped $CsPbCl_3$ nanocrystals driven by dynamic halogen exchange. *ACS Appl. Mater. Interfaces* **10**, 39872–39878 (2018).
27. Hebig, J.-C., Kühn, I., Flohre, J. & Kirchartz, T. Optoelectronic properties of $(CH_3NH_3)_3Sb_2I_9$ thin films for photovoltaic applications. *ACS Energy Lett.* **1**, 309–314 (2016).
28. Jain, S. M. et al. An effective approach of vapour assisted morphological tailoring for reducing metal defect sites in lead-free, (CH3NH3)3Bi2I9 Bismuth-based perovskite solar cells for improved performance and long-term stability, *Nano Energ.* **49**, 614–624 (2018).
29. Ju, M. G. et al. Cesium titanium (IV) bromide thin films based stable lead-free perovskite solar cells. *Joule* **2**, 1–11 (2018).
30. Sansom, H. C. et al. $AgBiI_4$ as a lead-free solar absorber with potential application in photovoltaics. *Chem. Mater.* **29**, 1538–1549 (2017).
31. Wei, F. et al. Synthesis and properties of a lead-free hybrid double perovskite: $(CH_3NH_3)_2AgBiBr_6$. *Chem. Mater.* **29**, 1089–1094 (2017).
32. Noel, N. K. et al. Lead-free organic–inorganic tin halide perovskites for photovoltaic applications, *Energy Environ. Sci.* **7**, 3061–3068 (2014).
33. Wang, J. et al. Highly efficient perovskite solar cells using non-toxic industry compatible solvent system. *Sol. RRL* **1**, 11 (2017).
34. Liang, J.-J. et al. Detrimental effect of silver doping in Spiro-OMeTAD on the stability and performance of perovskite solar cells. *Org. Electron.* **69**, 343–347 (2019).
35. Domanski, K. et al. Not all that glitters is gold: metal-migration-induced degradation in perovskite solar cells. *ACS Nano* **10**, 6306–6314 (2016).
36. Wang, H. et al. Fabrication of methylammonium bismuth iodide through interdiffusion of solution-processed BiI_3/CH_3NH_3I stacking layers. *RSC Adv.* **7**, 43826–43830 (2017).
37. Jeon., N. J. et al. Solvent engineering for high-performance inorganic-organic hybrid perovskite solar cells. *Nat. Mater.* **13**, 897–903 (2014).
38. Jain, S. M. et al. Frustrated Lewis pair-mediated recrystallization of $CH_3NH_3PbI_3$ for improved optoelectronic quality and high voltage planar perovskite solar cells. *Ener. Environ. sci.* **6**, 3770–3782 (2016).
39. Ren, S. et al. Inorganic-organic hybrid solar cell: bridging quantum dots to conjugated polymer nanowires. *Nano Lett.* **11**, 3998–4002 (2011).
40. Stoumpos, C. C., Malliakas, C. D. & Kanatzidis, M. G. Semiconducting tin and lead iodide perovskites with organic cations: phase transitions, high mobilities, and near-infrared photoluminescent properties. *Inorg. Chem.* **52**, 9019–9038 (2013).
41. Chen, Z., Wang, J. J., Ren, Y., Yu, C. & Shum, K. Schottky solar cells based on $CsSnI_3$ thin-films. *Appl. Phys. Lett.* **101**, 093901 (2012).

42. Pham, H. D. et al. Molecular engineering using an anthanthrone dye for low-cost hole transport materials: a strategy for dopant-free, high-efficiency, and stable perovskite solar cells. *Adv. Energy Mater.* **8**, 1703007 (2018).
43. DiPalma, J. R. Bismuth toxicity, often mild, can result in severe poisonings. *Emergency Med. News* **23**, 16–20 (2001).
44. Brabec, C. J. et al. Origin of the open circuit voltage of plastic solar cells. *Adv. Funct. Mater.* **11**, 374–380 (2001).
45. Ross, R., Nozik, A. Efficiency of hot-carrier solar energy converters, *J. Appl. Phys.* **53**, 3813–3818 (1982).
46. Gelmetti, I. et al. Energy alignment and recombination in perovskite solar cells: weighted influence on the open circuit voltage. *Energy Environ. Sci.* **12**, 1309–1316 (2019).
47. Gadisa, A., Svensson, M., Andersson, M. R. & Ingana¨s, O. Correlation between oxidation potential and open-circuit voltage of composite solar cells based on blends of polythiophenes/ fullerene derivative. *Appl. Phys. Lett.* **84**, 1609–1611 (2004).
48. Marin-Beloqui, J. M., Lanzetta, L. & Palomares, E. Decreasing charge losses in perovskite solar cells through mp-TiO2/MAPI interface engineering. *Chem. Mater.* **28**, 207–213 (2016).
49. Elumalai, N. K. & Uddin, A. Open circuit voltage of organic solar cells: an in-depth review. *Energy Environ. Sci.* **9**, 391–410 (2016).
50. Pham, H. D. et al. One step facile synthesis of a novel anthanthrone dye-based, dopant-free hole transporting material for efficient and stable perovskite solar cells. *J. Mater. Chem. C.* **6**, 3699–3708 (2018).
51. Scofield, J. H. J. Electron spectrosc. *Relat. Phenom.* **8**, 129–139 (1976).
52. Gorgoi, M. et al. Nuclear instruments and methods in physics research section A: accelerators, spectrometers. *Detect. Assoc. Equip.* **601**, 48–56 (2009).

Acknowledgements

This project has received funding from the European Union's Horizon 2020 research and innovation programme under the Marie Skłodowska-Curie grant agreement no. 663830. S.M.J. is thankful to Welsh assembly Government funded Sêr Cymru Solar project, EPSRC grants EP/M025020/1 and Supergen Super solar challenge and Marie-Curie COFUND fellowship for financial support.

Author contributions

S.M.J. conceived and designed the overall experiments, prepared devices, performed X-ray diffraction, X-ray photoelectron spectroscopy, Ultraviolet visible, photoluminescence measurements and analysis of data, and wrote the paper. T.E. made the symmetry structure for MBI films and participated in analysis and editing of the paper. J.R.D. participated in analysis and edited the paper.

Additional information

Supplementary information accompanies this paper at https://doi.org/10.1038/s42004-019-0195-3.

Competing interests: The authors declare no competing interests.

Reprints and permission information is available online at http://npg.nature.com/reprintsandpermissions/

Publisher's note: Springer Nature remains neutral with regard to jurisdictional claims in published maps and institutional affiliations.